lajss.org© Latin American Journal of Solids and Structures
www.lajss.org

Optimization of Vibration Band Gaps in Damped Lattice Metamaterials

Rubens Gonçalves Salsa Junior[a]*, Thiago de Paula Sales[b], Domingos Alves Rade[c]

[a] Universidade Federal do Rio Grande do Norte, Departmento de Engenharia Mecânica, Natal, RN 59078-970, Brasil. Email: rubens.salsa@ufrn.br
[b] Instituto Tecnológico de Aeronáutica, Divisão de Engenharia Mecânica, São José dos Campos, SP 12228-900, Brasil. Email: tpsales@ita.br
[c] Instituto Tecnológico de Aeronáutica, Divisão de Engenharia Mecânica, São José dos Campos, SP 12228-900, Brasil. Email: rade@ita.br

* Corresponding author

https://doi.org/10.1590/1679-78257486

Abstract

Recent research on structural dynamics has steered towards elastic metamaterials, as band gap phenomena can be explored to mitigate vibration. A challenge in their design is the determination of configurations resulting in wider band gaps in lower frequency ranges. Since some level of damping is unavoidable in any real engineering structure, it is necessary to extend the current methodology of optimal design to provide a deeper understanding of how damping may affect the desired performance. Therefore, the main objective of this article is to propose and evaluate a numerical procedure for the optimization of band gaps in damped metamaterials. Specifically, a modified objective function that incorporates an evanescence index integral is used and two optimization schemes are implemented, each reflecting whether the structure is undamped or damped. It is shown that the optimal damped metamaterial has wider range of attenuation than the undamped optimal one, but with decreased attenuation levels. The optimization procedure is validated numerically for a finite structure, demonstrating reduced transmissibility of wave motions.

Keywords

phononic crystals, band gaps, resonant metamaterials, optimization, damping, vibration control

Graphical Abstract

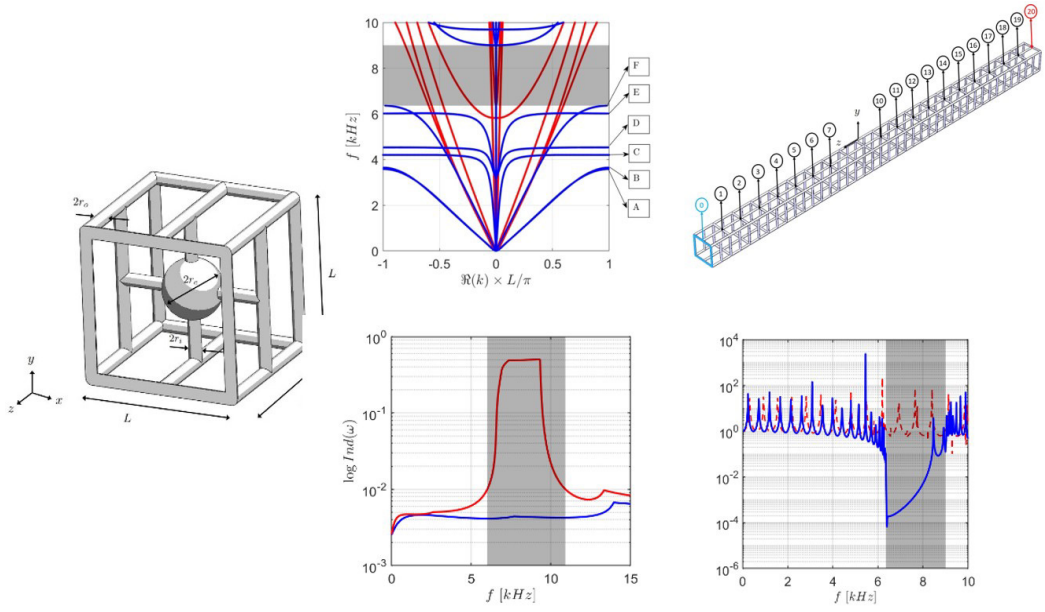

Received: January 27, 2023. In revised form: May 29, 2023. Accepted: June 05, 2023. Available online: June 05, 2023.
https://doi.org/10.1590/1679-78257486

1 INTRODUCTION

Metamaterials consist of structures constructed from a periodic repetition of identical substructures or unit cells, engineered to exhibit properties that are generally viewed to go beyond what one expects to find in naturally occurring or conventional materials. One of the most important features of metamaterials is the possible existence of frequency ranges, known as band gaps, within which the propagation of elastic waves in the structure is prohibited or only evanescent waves with spatial decay exist. It is not surprising that such wave filtering capability has rendered metamaterials appealing to a vast range of engineering applications demanding vibration mitigation.

The attenuation phenomenon induced by periodicity, named Bragg scattering, occurs when the wavelengths of traveling waves become twice the length of the unit cells, so that transmitted and reflected waves within the periodic media undergo destructive interference caused by impedance mismatches resulting from their deliberately designed alternating spatial properties (Vasileiadis et al., 2021). Because of the dependence on wavelength, which in turn is related to structural stiffness, Bragg band gaps tend to occur at relatively high frequencies. This can be a serious limitation for application in many engineering structures for which low-frequency range is of primary interest.

With the purpose of obtaining band gaps in lower frequency ranges, researchers have often resorted to the so-called elastic metamaterials. They consist of metamaterials whose unit cells contain resonators that act akin to a dynamic vibration absorber. Band gaps associated with local resonances are due to the out-of-phase motion of the base structure with respect to the internal resonators, where the energy of elastic waves is absorbed by the resonators. Resonant-type band gaps have been extensively studied recently and this concept has been validated for rods (Xiao et al., 2012), beams (Miranda Jr. and Dos Santos, 2019) and plates (Miranda Jr. et al., 2019). In addition, there are a variety of options for designing resonating unit cells and they usually contain holes (Wang and Wang, 2013), inclusions (Matlack et al., 2016) or pillars (Gao et al., 2019). These applications show the potential for tunability of internal resonances, which can leverage the local resonance mechanism between the unit cell and the auxiliary oscillators to ensure a variety of functional improvements with respect to the corresponding resonator-free periodic structure, evidencing that resonating elastic metamaterials can provide transmissibility reduction of elastic waves, with potential use, for example, as support structures, where vibration isolation is an essential property.

While research on elastic metamaterials mostly focuses on obtaining dispersion relations and analyzing the effect of local resonator design parameters on band gap width and location, a challenging issue arises when obtaining new configurations that result in wider band gaps in lower frequency ranges. This represents an aspect of paramount importance in design because the larger the band gap, the more flexible the manipulation of the elastic waves is. Because of the nontrivial interplay between different components in complex engineering systems, this task has been tackled with the systematic implementation of optimization procedures to determine the optimal design of metamaterials and local resonators for some types of structures. Hussein et al. (2006) used a multi-objective genetic algorithm to design one-dimensional periodic unit cells targeting frequency band structures characterizing longitudinal wave motion. Later, Hussein et al. (2007) again used genetic algorithms to obtain broadband frequency isolation in a bi-material two-dimensional unit cell. Gazonas et al. (2006) also utilized a genetic algorithm to maximize the relative acoustic band gap. Liu and colleagues (2014) implemented a two-stage design method, based on genetic algorithm in conjunction with fast plane wave expansion method, to carry out the topology optimization and determine a configuration that maximized relative band gap between two prescribed dispersion branches. Vatanabe et al. (2014) maximized the width of absolute elastic wave band gaps in piezocomposite materials by means of topology optimization. Romero-García et al. (2009) used stochastic search procedures based on evolutionary algorithms to determine the optimal distribution of holes for effectively controlling sound waves. Abedi and Mirjalili (2015) utilized particle swarm optimization algorithm to find the optimum structure of a corrugated metamaterial. Jung et al. (2020) used topology optimization for designing a local resonator in order to tailor flexural band gaps in plate structures. Bacigalupo et al. (2017) combined anti-chiral lattice structure with inertial resonators, and designed the number, arrangements, and material properties of the resonators to improve band gap properties using a nonlinear optimization algorithm. Later, Bacigalupo et al. (2019) successfully utilized machine-learning techniques for the spectral optimization of a tetrachiral metamaterial. Dal Poggetto et al. (2019) obtained an optimal resonator distribution in a tall building to maximize the width of the formed band gap for a given beam and a frequency range of interest using the GlobalSearch function from Matlab. Recently, a sequential quadratic programming algorithm was used to solve a constrained nonlinear optimization problem (Dal Poggetto et al., 2021; Dal Poggetto and Arruda, 2021) to obtain solutions that maximize an objective function capable of yielding low-frequency band gaps in a plate and to design spider web-inspired single-phase phononic crystals through selective variation of thread radii and the addition of point masses, respectively. From the technological viewpoint, a successful optimization of the dispersion properties for elastic metamaterials paves the way for developing a new generation of smart engineering structures, besides overcoming the difficulties in determining design variables that contribute to open band gaps.

A common characteristic in these research works is that models for metamaterials under consideration have no damping mechanism. When damping is not present, the attenuation zones, characterized with dispersion diagrams, are related to the presence of frequency regions where wave numbers have non-zero imaginary parts. This is because imaginary wave numbers represent evanescent (non-propagating) wave modes, and complex wave numbers are associated with propagating wave modes for which attenuation will occur after the wave travels over a few unit cells. The clear advantage of neglecting damping is this effortless identification of band gaps, which readily provides straightforward means of implementation in optimization routines. In contrast, all frequency-dependent wave numbers are complex-valued when any level of damping is included in the model. In such instances, all wave modes have some level of spatial decay, and the usual concept of band gap now must be exchanged to that of a zone of strongly attenuated wave propagation. This creates an obvious difficulty in determining the edge frequencies of a band gap, and several researchers have proposed alternatives. Chen et al. (2019) used the minimum imaginary component of all wave numbers at a given frequency, while Krushynska et al. (2016) utilized an effective loss factor. Collet et al. (2011) utilized an evanescence ratio index, which is the minimum imaginary component normalized by wave number absolute value. Pierce and Matlack (2021) developed an ingenious evanescence indicator for elastic metamaterials with one-dimensional periodicity that relates the decay component of the wave vector to the transmitted wave amplitude through a finite structure. The proper identification of band gaps is not the only difficulty imposed by the inclusion of dissipation. Damping has also been shown to significantly affect the operation of elastic metamaterials, broadening the width of band gap at the cost of a decreased peak attenuation performance (Van Belle et al., 2017), as well as curtailing attenuation at times (Aladwani and Nouh, 2020). In addition, damping can make multiple band gaps to coalesce (Xiao et al., 2019), create wave number band gaps (Frazier and Hussein, 2012) and induce branch overtaking in dispersion curves (Hussein and Frazier, 2010).

Since some level of damping is unavoidable in any real engineering structure, due, for example, to the inherent characteristics of the materials or the presence of friction, it is necessary to extend the current methodology of optimal design to damped elastic metamaterials, providing a deeper understanding of how damping may affect the desired performance. From the perspective presented herein, the main objective of this article is to optimize band gaps in damped resonating metamaterials. Specifically, a modified objective function that incorporates an evanescence index integral is used to obtain optimal band gaps. This modification is needed to generate zones of strong attenuation, a determining factor to characterize band gaps in damped metamaterials. The methodology presented herein is applied to a three-dimensional lattice metamaterial whose unit cell is conceived so that it can feature a resonator formed by a sphere connected to an elastic suspension. It is modeled by the finite element method, which enables to consider its complicated geometry, and wave modes are obtained by considering Floquet-Bloch periodicity conditions. The differences in methodologies with respect to optimizing the corresponding undamped structure are highlighted throughout the text. Band gaps for the associated undamped structure are identified by inspecting the corresponding dispersion relation, while an evanescence index is used when damping is accounted for. Furthermore, it is shown that the optimal damped structure has a wider range of attenuation than the undamped optimal one, but with decreased peak of attenuation. Finally, the methodology is validated for a finite structure, comprising a finite number of unit cells, showing that the optimized lattice metamaterial can have decreased transmissibility of mechanical waves over a wide range of frequencies when compared to its resonator-free counterpart. Even though the methodology presented herein is general and applicable to other forms of dissipation, such as viscous damping, only structural damping is considered.

This paper is organized as follows: the structures under investigation are expounded in Section 2. Their wave propagation characteristics, considering the undamped and damped cases are discussed in Section 3. The optimization formulation is presented in Section 4. Results are presented in Section 5, followed by the concluding remarks in Section 6.

2 MODEL FOR A THREE-DIMENSIONAL LATTICE METAMATERIAL

Recently, there has been an increased tendency to use spatially sparse geometries to design systems capable of yielding large attenuation bands (Dal Poggetto et al., 2021), specially due to the ease in constructing structures with complex geometries using additive manufacturing (Jia et al., 2018). Consequently, the three-dimensional lattice structure shown in Fig. 1a was adopted as the baseline unit cell investigated in this work. It consists of a cubic grid of size L, "outer" beam-like members, whose cross-sections are circular, with radius r_o. Additional beam-like struts are placed inside the cuboidal shape, to form a cross; these "inner" beams also have circular cross-section, with radius r_i. To introduce an alternative version featuring a resonator, inspired by the design of Elmadih et al. (2019), a solid sphere of radius r_e is added to the center of the unit cell, as shown in Fig. 1b. This unit cell is conceptualized in a manner so that the sphere supported by the flexible inner beams can function as a local resonator. Both structures can be used in a variety of

applications due to their high stiffness and large surface-to-volume ratio, while their band gap properties reveal potential applications in vibration isolation as support structures. In addition, the stiffness and mass properties of the unit cells can be easily parameterized to enable optimization according to design goals.

Since one-dimensional periodicity is common to many structures in engineering, it is assumed the infinite structure has translational periodicity along the z direction, as depicted in Fig. 1c (only the version with internal resonators is shown). Additionally, it is assumed that wave propagation is approximately one dimensional, i.e., waves propagate along the z direction, whilst propagation in transverse directions is not considered. This hypothesis is not at all restrictive, since wave modes in z direction still involve the propagating and evanescent modes of longitudinal, bending, torsional and shear types.

The unit cells are modeled using the finite element method. Initially, the unit cell was discretized with three-dimensional quadratic tetrahedral elements, a typical finite element mesh is illustrated in Fig. 1d for the unit cell featuring the resonator. However, exorbitant computational costs in simulations lead to a simplified model in which the structural frames were modeled according to Timoshenko beam theory, which is capable of capturing transverse shear deformation effects. In addition, the central sphere was modeled as a rigid solid sphere connected to the inner beams.

3 COMPUTATION OF BAND STRUCTURES

The wave modes of the considered lattice structures were computed using the wave-based finite element method, which is an attractive technique when modeling complex structures, for which analytical solutions might not be readily available (Mencik, 2010). In this manner, only the finite element model of a unit cell is needed, which is combined with Bloch's theorem and Floquet boundary conditions along the interfaces (Collet et al., 2011). Consequently, a hybrid approach, that involves computing the mass and stiffness matrices via commercial packages, can be seamlessly implemented.

The method adopted for the modeling of one-dimensional periodic structures is concisely explained as follows: a finite element model of a unit cell is constructed and the mass $\mathbf{M}$ and stiffness $\mathbf{K}$ matrices are computed. For consistency, care must be exercised to ensure that, with respect to Fig. 1c, left-hand and right-hand boundaries of each unit cell along z direction must contain the same set of degrees-of-freedom. The dynamic equations of motion of a unit cell are expressed in the frequency domain as

$$\mathbf{D}\mathbf{q} = \mathbf{f}, \tag{1}$$

where $\mathbf{q}$ and $\mathbf{f}$ represent n-dimensional vectors of generalized displacements and forces, respectively. Here,

$$\mathbf{D} = (1 + i\eta)\mathbf{K} - \omega^2\mathbf{M} \tag{2}$$

is the $n \times n$ dynamic stiffness matrix of a unit cell, ω is the circular frequency and η is the constant structural damping loss factor. Structural damping is considered due to its simplicity, but $\mathbf{D}$ may be appropriately modified to include viscous damping or any other linear damping model. In this case, the structure is undamped when $\eta = 0$.

The degrees of freedom can be decomposed into internal, left (subscript *L*) and right (subscript *R*) boundaries. Assuming that there are no external forces acting on the interior degrees-of-freedom, Eq. (1) is reformulated in terms of state vectors comprised by the quantities pertaining the left and right boundaries as

$$\mathbf{u}_R = \mathbf{S}\mathbf{u}_L, \tag{3}$$

where

$$\mathbf{u}_R = \begin{bmatrix}\mathbf{q}_R \\ \mathbf{f}_R\end{bmatrix} \text{ and } \mathbf{u}_L = \begin{bmatrix}\mathbf{q}_L \\ \mathbf{f}_L\end{bmatrix}. \tag{4}$$

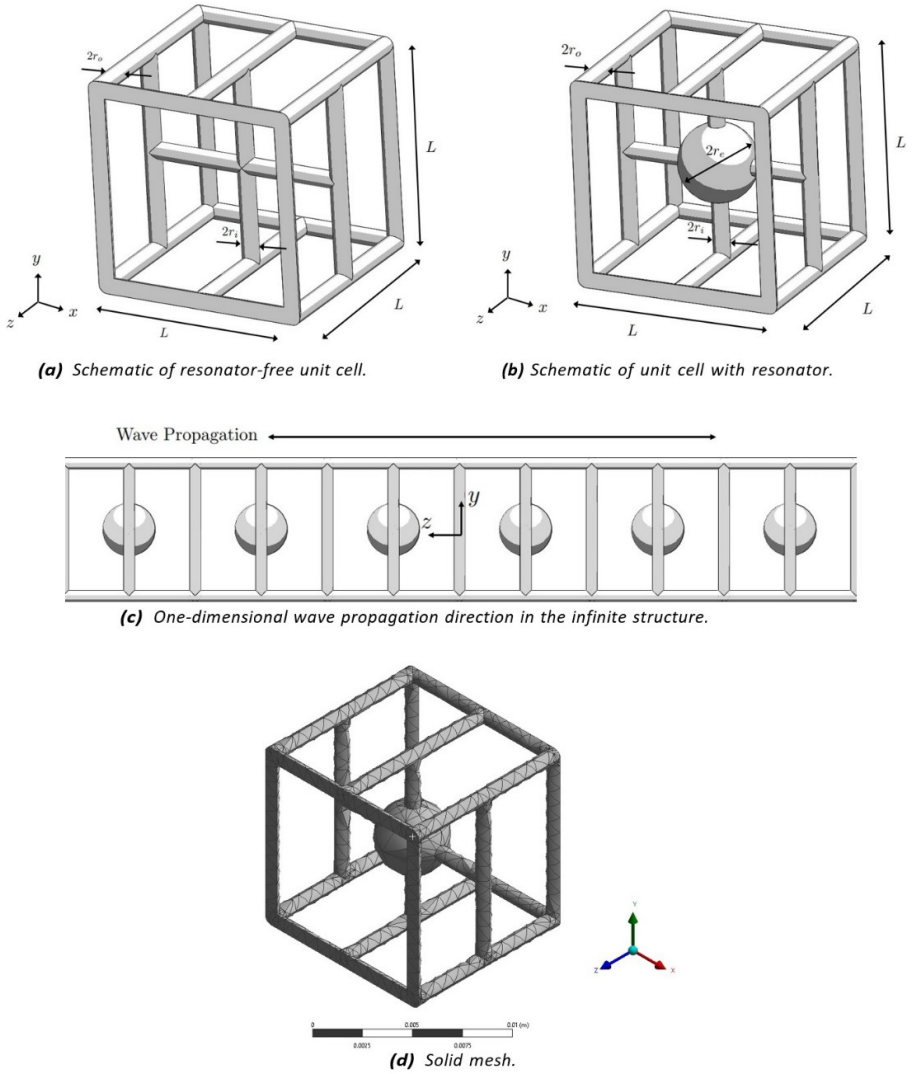

(a) *Schematic of resonator-free unit cell.*

(b) *Schematic of unit cell with resonator.*

(c) *One-dimensional wave propagation direction in the infinite structure.*

(d) *Solid mesh.*

Figure 1: Unit cells of length L. Both outer and inner beams have circular cross-sections, with radii r_o and r_i, respectively. The sphere has radius r_e.

Here, $\mathbf{S}$ is a $2n \times 2n$ symplectic matrix composed of sub-blocks of the dynamic stiffness matrix condensed onto its left and right boundaries. Periodicity along the propagation direction implies the coupling condition between two consecutive unit cells m and $m-1$, i.e.:

$$\mathbf{u}_L^{(m)} = \mathbf{u}_R^{(m-1)}. \tag{5}$$

This condition, combined with Eq. (3), yields

$$\mathbf{u}_L^{(m)} = \mathbf{S}\mathbf{u}_L^{(m-1)}. \tag{6}$$

The solutions of Eq. (6) must be of the form $\mathbf{u}_L^{(m)} = \mu \mathbf{u}_L^{(m-1)}$, according to Bloch's theorem. While this yields the eigenvalue problem $\mathbf{S}\mathbf{u}_L^{(m-1)} = \mu \mathbf{u}_L^{(m-1)}$in the physical displacement/force vector $\mathbf{u}_L^{(m-1)}$, it can be recast in the form

$$\mathbf{S}\boldsymbol{\phi} = \mu \boldsymbol{\phi}, \tag{7}$$

where $\boldsymbol{\phi}$ is an eigenvector. The scalar parameter μ is related to the wave number k through the relation

$$\mu = e^{-ikL}, \tag{8}$$

while the corresponding $2n$-dimensional vector $\boldsymbol{\phi}$ gathers information concerning the wave mode shapes, related to the spatial distribution of the displacements and internal forces over the cross-section of the unit cell along its boundaries. Here, L is the length of the unit cell in the direction of wave propagation. For clarification purposes, one should mention that, for determining dispersion relations, an alternative eigenproblem has been considered ($\mathbf{S}+\mathbf{S}^{-1}$approach), instead of the one presented above in Eq. (7), which is known to be prone to numerical issues such as ill-conditioning. Information regarding this matter can be found in the work of Zhong and Williams (1995).

Band gaps can be readily identified for the undamped structure. Since k must be real for purely propagating waves, zones of attenuation can be detected from the dispersion relations $\mathbf{k}(\omega)$ at the frequency range where all wave numbers have non-zero imaginary part. However, in the case where dissipation is present, all wave numbers are complex, and the situation is less clear. A method for identifying band gaps that is useful for implementation in optimization routines involves the use of an indicator of minimal evanescence ratio of all computed waves for each considered frequency, defined as (Collet et al., 2011)

$$\mathrm{Ind}(\omega)=\min_{j}\left\{\frac{|\Im[k_j(\omega)]|}{|k_j(\omega)|}\right\}, \tag{9}$$

where $\Im[k_j(\omega)]$ is the imaginary part of j-th wave number $k_j(\omega)$ and $|\cdot|$ indicates an absolute value. To determine whether $\mathrm{Ind}(\omega)$ represents a zone of strong attenuation (band gap) at ω, it is necessary to introduce a threshold value, here denoted as Ind_T: if $\mathrm{Ind}(\omega)>\mathrm{Ind}_\mathrm{T}$, then there is a band gap at ω. The specified value for Ind_T is arbitrary and needs to be selected on a case-by-case basis. For the structure under consideration, it is specified in Section 5.3.2.

4 FORMULATIONS OF THE OPTIMIZATION PROBLEM

To obtain a band gap that is as wide as possible at the lowest possible frequency range, the values of a previously chosen set of geometric design parameters can be determined by formulating an appropriate optimization problem. For periodic structures, common strategies that have been used to achieve this goal involve variations of cross-sections in specific regions (Bibi et al., 2019; Dal Poggetto and Arruda, 2021; Dal Poggetto et al., 2021) and exploration of the effect of local resonance (Claeys et al., 2016; Miranda Jr. et al., 2019; Gao et al., 2019; Dal Poggetto et al., 2021).

In the approach followed here, the design parameters chosen for band gap optimization are those directly linked with the internal oscillator. In particular, the radius of the internal beams, r_i, and the radius of the sphere, r_e, were considered as the two design variables. The radius of the sphere r_e impacts the mass of the local resonator and the radius of the internal beams r_i is a measure of the stiffness for the resonator. It should be noted that there is additional coupling between the radius of the sphere and the stiffness provided by the internal beams, since their length is directly impacted by the presence of the sphere. Other parameters could have been chosen as well, such as the material's mass density or Young's modulus. However, attention has been restricted to geometrical parameters of the resonator because, in this way, the obtained designs might be more easily physically realizable. For the same reason, the radii of the four internal beams were set to vary as one, and not independently.

In the optimization, the considered parameters are not entirely free to vary, being subjected to constraints. For simplicity, the radius of the internal beams is restricted to lie in the range $r_i\in(0,r_o]$, where the upper limit r_o represents the radius of beams forming the outer frame of the structure. In practice, the lower limit should be restricted to the minimal radius possible for the chosen manufacturing process, if such structure was to be physically realized. The radius of the sphere can be restricted to lie in any range $r_e\in(0,R_{\max}]$, where $R_{\max}<L/2$, so that the sphere is always encased by the outer frame, and the lower limit characterizes a structure without a resonator.

In a similar optimization setting, success has been achieved by Han and Zhang (2019) and Dal Poggetto and Arruda (2021) using an objective function that involves the ratio between the band gap mean frequency and its width, which is the strategy adopted here, for which the optimization problem consists in:

$$\min_{r_e,r_i} f_{\mathrm{obj}}^{(1)}=\min_{r_e,r_i}\frac{(\omega_u+\omega_l)/2}{(\omega_u-\omega_l)}, \tag{10}$$

where ω_l and ω_u are the lower and upper frequency limits of a band gap. The purpose of $f_{\mathrm{obj}}^{(1)}$ is to maximize $\omega_u-\omega_l$ to obtain a band gap that is widest as possible, while at the same time minimizing its central frequency $(\omega_u+\omega_l)/2$.

While the objective function $f_{\mathrm{obj}}^{(1)}$ is adequate to perform optimization of band gaps observed in undamped periodic structures, it needs to be modified to accommodate systems with damping. This is necessary because application of (10)

to a damped system may result in large attenuation zones, but whose intensity of attenuation might not be great enough to characterize an effective band gap. This issue can be circumvented by utilizing the modified objective function

$$\min_{r_e,r_i} f_{\text{obj}}^{(2)} = \min_{r_e,r_i} \frac{(\omega_u+\omega_l)/2}{(\omega_u-\omega_l)\int_{\omega_l}^{\omega_u} \text{Ind}(\omega)d\omega}. \tag{11}$$

Here,

$$\int_{\omega_l}^{\omega_u} \text{Ind}(\omega)d\omega \tag{12}$$

is the area under the curve representing $\text{Ind}(\omega)$in the interval (ω_l, ω_u). This simple adjustment guarantees that the attenuation in the interval (ω_l, ω_u) is significantly more intense than in other frequency bands being considered.

5 RESULTS

5.1 Dispersion characteristics of the lattice structure

To obtain a Before applying the optimization procedure, the unit cell is initially defined with the dimensions $L = 10$ mm, $r_o = 0.42$ mm, $r_i = 0.42$ mm and $r_e = 2$ mm. It is composed of structural steel, with density $\rho = 7850$ kg/m^3, Poisson ratio $\nu = 0.3$, and Young's modulus $E = 200$ GPa. The proceeding analysis will focus on the frequency zone 0 − 10 kHz.

5.1.1 Undamped Structure

Firstly, the undamped unit cell is considered ($\eta = 0$ in Eq. (2)). As mentioned before, the first attempt was to discretize the unit cell with 3D quadratic tetrahedral elements, but exorbitant computational costs in simulations lead to the option for a simplified model which adopts Timoshenko theory for the modeling of the beams as well as a solid rigid body to model the sphere at the center of the unit cell. Fig. 2 enables to compare the dispersion relation for propagating wave modes computed with the two models. The 3D model with local resonator is composed of 27102 degrees of freedom while its resonator-free counterpart has 26079. On the other hand, the simplified model has 6414 and 5694 degrees of freedom, corresponding to both configurations, respectively. The dispersion curves for the structure with internal local resonators (Fig. 2a) and the resonator-free structure (Fig. 2b) are computed using the wave-based finite element method. Despite small discrepancies due to the different features of both models, the diagrams show reasonably good agreement regarding the behavior of wave modes, which were obtained at reduced computational cost for the simplified model. Therefore, the adoption of the simplified model can be justified, and was used to obtain the results shown in the remainder of this article. It should be noted that the structures do not have complete band gaps in the frequency range shown, suggesting that an optimization problem should be be posed in order to open up and maximize band gaps of all wave modes.

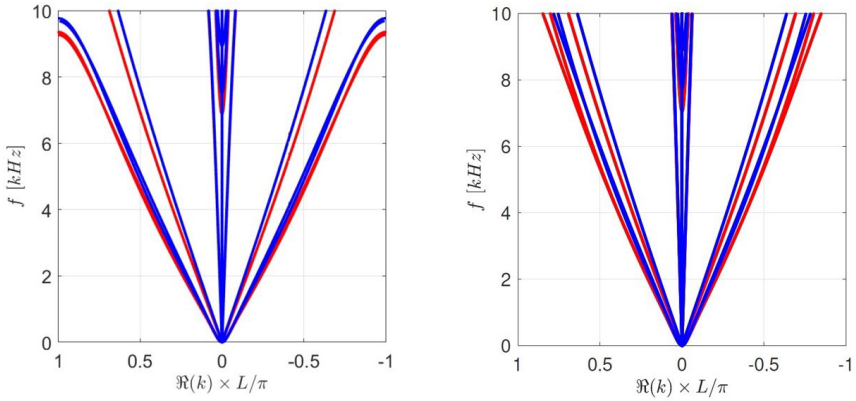

(a) *Unit cell with local resonator.* ***(b)*** *Resonator-free unit cell.*

Figure 2: Comparison of dispersion diagrams for the initial design of the lattice structures obtained with the 3D finite element model using quadratic tetrahedral solid elements (●) and the simplified Timoshenko beam model (●). Figure shows only propagating wave modes and $\Re(\omega)$ stands for the real part of k.

Even though the interest is confined to waves propagation in the z direction, the dispersion diagrams indicate the existence of a full set of wave modes propagating in other directions as well. For example, the four wave modes propagating at 2 kHz are shown in Fig. 3 for both structures. There are two bending wave modes (with respect to axes x and y), a longitudinal wave mode along z, and a torsional mode. Ideally, a complete band gap could extinguish propagation of these four modes.

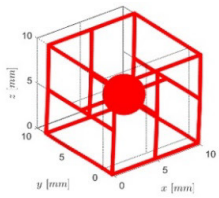

(a) *First bending wave mode for structure with resonator.*

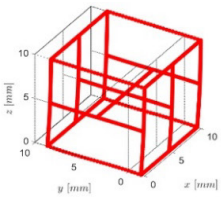

(b) *First bending wave mode for resonator-free structure.*

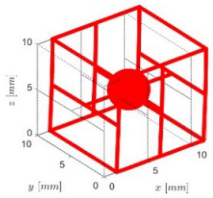

(c) *Second bending wave mode for structure with resonator.*

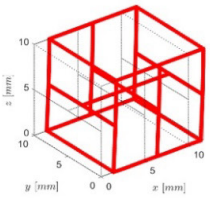

(d) *Second bending wave mode for resonator-free structure.*

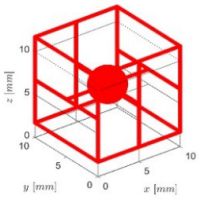

(e) *Longitudinal wave mode for structure with resonator.*

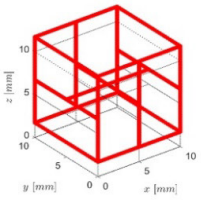

(f) *Longitudinal wave mode for resonator-free structure.*

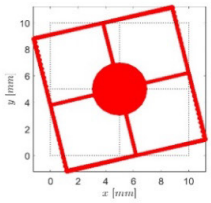

(g) *Torsional wave mode for structure with resonator.*

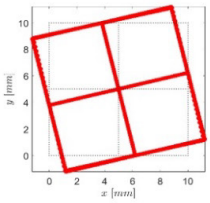

(h) *Torsional wave mode for resonator-free structure.*

Figure 3: Propagating wave modes for $f = 2$ kHz. The unit cell initial configuration is plotted in gray, and the wave mode-related displacements are plotted in red.

5.1.2 Damped Structure

Next, structural damping is considered by means of $\eta \neq 0$ in Eq. (2). To accentuate any influence it may have, a structural damping factor of $\eta = 1\%$ was utilized in this paper, which is considered high for aluminum. Wave numbers were still determined with the wave-based finite element method, but dispersion diagrams should now be replaced with analysis of evanescence indicator in Eq. (9). The evanescence indicator for the initial design is shown in Fig. 4. It can be seen that, because of damping, waves are attenuated at all frequencies, but both resonator-free and resonant structures do not have band gaps because there are no zones of strong wave attenuation, specially when compared with the results from Section 5.3.2.

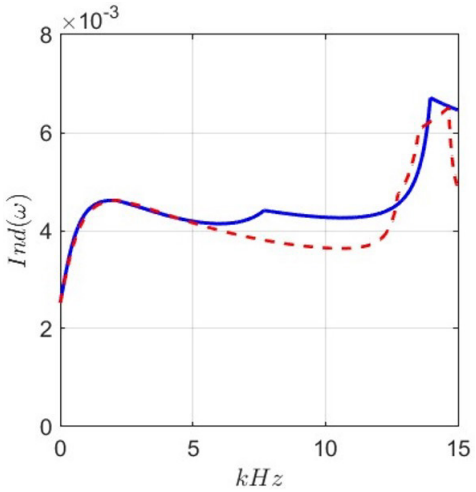

Figure 4: Evanescence indicator for initial design of dissipative structures with resonators (—) and without resonators (---).

5.2 Parametric analysis of band gap formation

The design parameters chosen for band gap optimization are those directly linked with the internal oscillator, composed of the rigid sphere and internal beams attached to the sphere. In particular, the radius of the internal beams, r_i, and the radius of the sphere, r_e, are considered as the two design variables. The interest is to appraise how r_i and r_e affect the band gap formation for the undamped and damped cases in the interval 0-10 kHz.

5.2.1 Undamped structure

Firstly, the undamped system is considered. Fig. 5 shows the location of complete band gaps for different values of r_i and r_e, i.e., band gaps that encompass all wave modes simultaneously. These correspond to regions where the all wave numbers have non-zero imaginary parts, thus corresponding to non-propagating waves. Firstly, the radius of the sphere is assumed to be given by $r_e = 3.766$ mm, while r_i is varied in the range $(0,0.42]$ mm. This upper limit is equal to the radius r_o of the outer beams. The constant value of r_e is arbitrarily chosen, with the restriction that band gaps can be observed in the investigated frequency range when r_i is swept. It is shown that the band gap is the widest for an intermediate value of r_i. Furthermore, increasing or decreasing the value of r_i shifts the band gap to the right or left, respectively, and it becomes narrower, until no band gap is observed (situation not shown in the figure).

Similarly, the radius of the internal beams is also held constant, $r_i = 0.145$ mm, while r_e is varied within the range $(0,4]$ mm. Now, this upper limit is imposed as a size restriction since the edges of the unit cell have length $L = 10$ mm. Fig. 5 shows that band gaps are wider for larger values of r_e, and that the band gap frequency range is shifted to the right. It is also interesting to note that, if r_e is not large enough, band gaps might not appear at all.

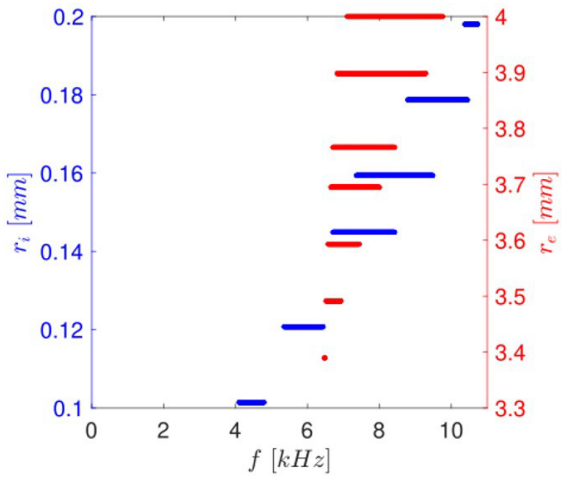

Figure 5: Parametric analysis of complete band gap formation for the undamped unit cell with resonator. Each solid line represents the frequency span of a band gap, where all wave numbers have non-zero imaginary part. Red lines are associated with the axis on the right, and are obtained by varying r_e, taking $r_i = 0.145$ mm. Blue lines are associated with the axis on the left, and are obtained by varying r_i, assuming $r_e = 3.766$ mm.

5.2.2 Damped structure

When damping is included, a parametric analysis can be carried out utilizing the objective function (11). Fig. 6a shows how $f_{\text{obj}}^{(2)}$ varies when $r_i = 0.145$ mm and r_e is swept in the same range considered previously in Fig. 5. Similarly, Fig. 6b shows how this objective function varies when $r_e = 3.766$ mm and r_i is swept in the same range shown before. Fig. 6 shows that zones of strong attenuation can be created with larger values of r_e and an intermediate value of r_i. These trends follow what has been observed for the influences of r_e and r_i on the band gap formation when damping was not considered, which is not surprising.

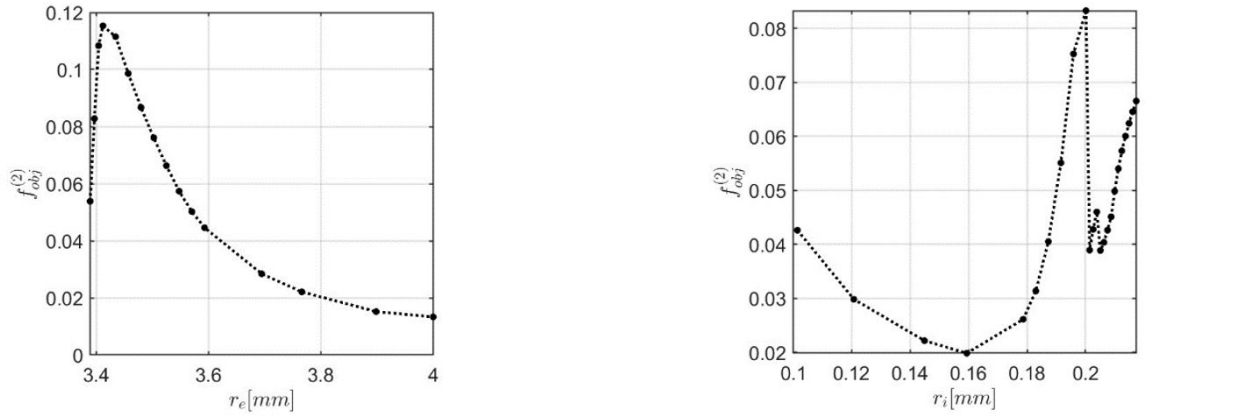

(a) *Variation due to r_e when $r_i = 0.145$ mm.* ***(b)*** Variation due to r_i when $r_e = 3.766$ mm.

Figure 6: Parametric analysis of the variation of for the case of damped structure.

5.3 Optimization of the unit cell

As can be noticed in Fig. 5 and Fig. 6, the individual influences of variations of the two design parameters are distinct from each other, which indicates the interest of using numerical optimization to obtain the optimal design of the resonant metamaterial. The optimization will aim at obtaining the largest band gap at the lowest frequency range possible inside the frequency zone 0-10 kHz. The optimization procedures and corresponding results are presented next.

5.3.1 Undamped structure

This minimization problem expressed by Eq. (10) is now to be solved. During the optimization, the radius of the internal beams was restricted to lie in the range $r_i \in (0,0.42]$ mm, where the upper limit 0.42 mm represents the radius of the outer beams. The radius of the sphere was restricted to lie in $r_e \in (0,4]$ mm. The upper limit of 4 mm is due to size constraints since the edges of the unit cell have length $L = 10$ mm.

Optimization was carried out using the differential evolution method, which has emerged as one of the most frequently used algorithms for solving complex optimization problems (Bilal et al., 2020). It is a meta-heuristic technique that follows the concepts of the theory of the evolution of species and can be separated in two phases: initialization and evolution. In the first phase, a set of N uniformly distributed population members are generated randomly in the search space. In the next phase, the generated population undergoes mutation, crossover, and selection processes.

It should be noted that the dispersion relation is computed with the wave-based finite element method for each new population member created. This process is repeated until a termination criterion is met. If the optimization is carried in the frequency interval $[\omega_1, \omega_2]$, the termination criteria is that either $\omega_l = \omega_1$ and $\omega_u = \omega_2$, or that the best and worst solutions found in a population (determined by the values of $f_{\text{obj}}^{(1)}$) satisfy

$$\Delta = 100 \times \frac{\text{worst} - \text{best}}{\text{best}} < 1. \tag{13}$$

Because damping is neglected, a penalization procedure is implemented in which population members that do not correspond to band gaps are associated with $f_{\text{obj}}^{(1)} \to \infty$. The algorithm is initialized with $N = 20$ population members, and the frequency range analyzed is 0-10 kHz, discretized in steps of 5 Hz. Due to the random nature of the employed optimization methodology, 10 runs are performed, and the best solution among them (smallest value of $f_{\text{obj}}^{(1)}$) is stored.

However, it might be theoretically possible to obtain smaller values of $f_{\text{obj}}^{(1)}$ if more runs are performed so, in this respect, only a locally optimal solution is computed. Fig. 7 shows that the algorithm converges after 43 iterations. The optimal values found are $r_i = 0.132$ mm and $r_e = 4$ mm.

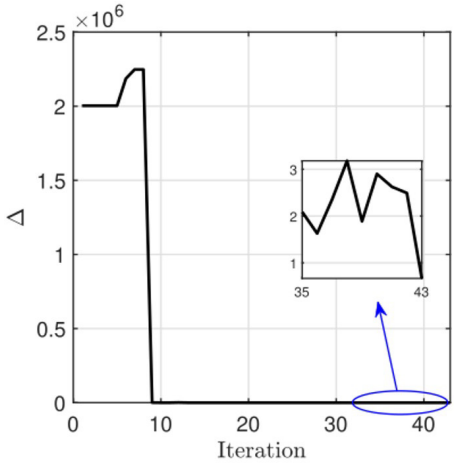

Figure 7: Convergence of differential evolution algorithm. The difference Δ between the best and worst solutions found in a population is given in logarithmic scale.

Fig. 8 shows the corresponding dispersion relation for the optimal periodic structure with local resonators. It is shown that no elastic waves can propagate in the range 6360-9006 Hz, which characterizes a complete band gap for all wave modes. It can also be seen that partial band gaps for specific wave types can be wider because they start at lower frequencies. For example, the band gaps for the two bending wave modes start at 3585 Hz and 3645 Hz. Similarly, the band gap for the longitudinal wave mode starts at 4202 Hz. The effect of the resonator is also evidenced when comparing this dispersion relation with that of the resonator-free structure, also shown in Fig. 8. The resonator-free structure possesses no band gaps in the frequency region shown. It is worth noting that the optimized structure has increased mass when compared to the originally designed unit cell: the initial design had mass of 8.063 g, while the optimized resonant structure has 26.023 g. This evidences the fact that the inertia of the oscillator must be increased in order to amplify its effectiveness in lowest frequency range possible and generate the widest band gap. Certainly, this result was expected but might not be applicable to instances when there are severe constraints on the added mass.

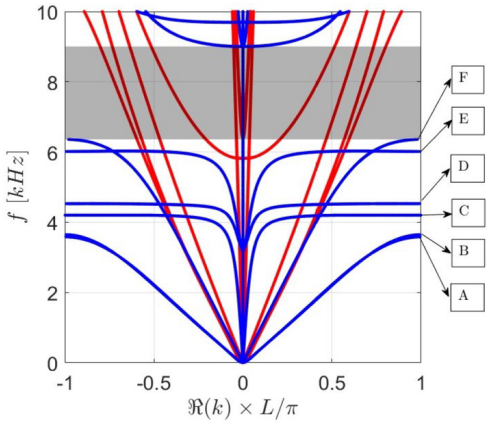

Figure 8: Dispersion curves for undamped periodic structure with local resonators (●) and resonator-free undamped lattice structure (●) with optimal dimensions for the resonator. Complete band gap for the optimal undamped metamaterial is marked with a shaded area.

In order to investigate the mechanism of band gap formation, the band gap opening modes, labeled from A to F in Fig. 8, are plotted in Fig. 9. To serve as a reference, the undeformed unit cell is outlined in black. It can be observed that, in modes A-C, the resonator vibrates out-of-phase with respect to the outer beam structure. At the same time, the oscillator vibrates profusely while the outer beam structure is comparatively motionless in modes D-F. These represent typical behaviors of locally resonant elastic systems (Baravelli and Ruzzene, 2013; Liu et al., 2000; Zhang et al., 2015).

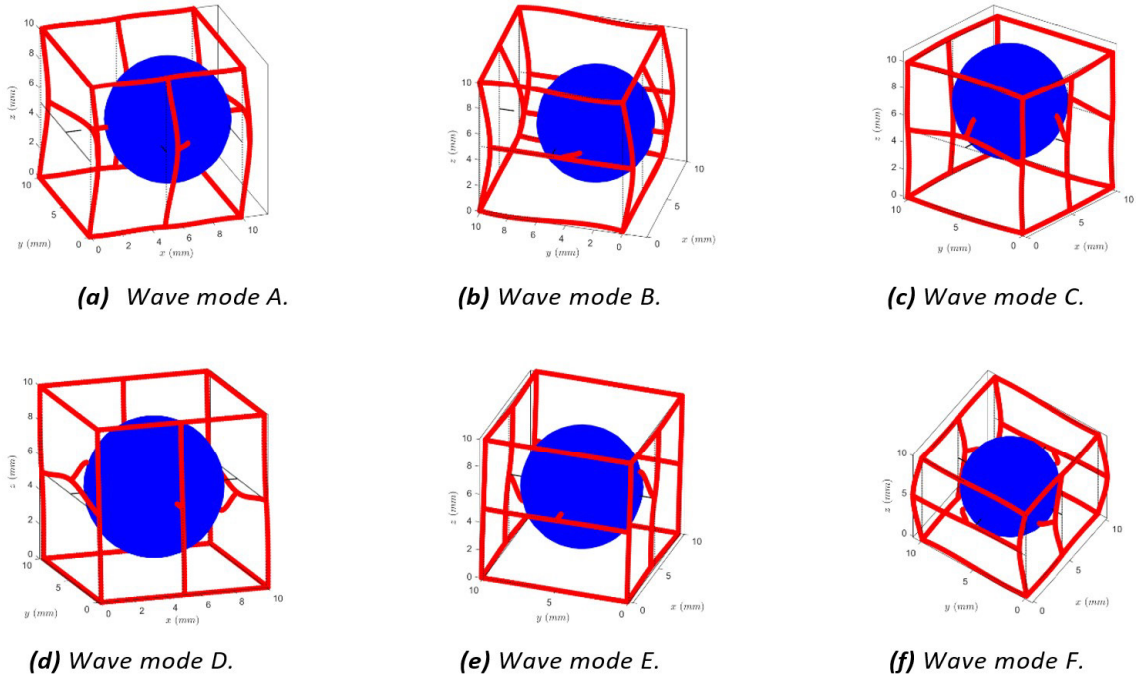

(a) *Wave mode A.* ***(b)*** *Wave mode B.* ***(c)*** *Wave mode C.*

(d) *Wave mode D.* ***(e)*** *Wave mode E.* ***(f)*** *Wave mode F.*

Figure 9: Wave modes at the lower boundaries of band gaps of the optimized undamped metamaterial, plotted as nodal displacements. The sphere is plotted in blue to facilitate visualization. Refer to Fig. 8 for labels A-F.

5.3.2 Damped structure

Now, attention is directed to the minimization problem expressed by Eq. (11). For the damped structure, the optimization algorithm is applied similarly to the undamped case. The main difference lies in the use of the evanescence index (9) and the call for the procedure to determine a band gap. As pointed out in Section 3, a threshold value Ind_T needs to be defined such that a band gap is present in the range $[\omega_1, \omega_2]$ when $\mathrm{Ind}(\omega) > \mathrm{Ind}_\mathrm{T}$. There is no universal way to determine Ind_T, so its value was chosen in a *ad hoc* manner. Different scaling factor $p > 0$ were tested in

$$\mathrm{Ind}_\mathrm{T} = p\% \cdot \left[\max_{\omega} \mathrm{Ind}(\omega) - \min_{\omega} \mathrm{Ind}(\omega)\right] \tag{14}$$

If p is too small, computing Ind_T over many generations could lead the optimization scheme to converge to a structure with large frequency range of attenuation but of low intensity, which does not characterize an actual band gap. On the other hand, if p is too large, no band gaps may be found. Therefore, it was found that $p = 2$ yielded satisfactory results for the metamaterial under consideration. With the same running conditions as before, Fig. 10 shows that the algorithm converged after 27 iterations.

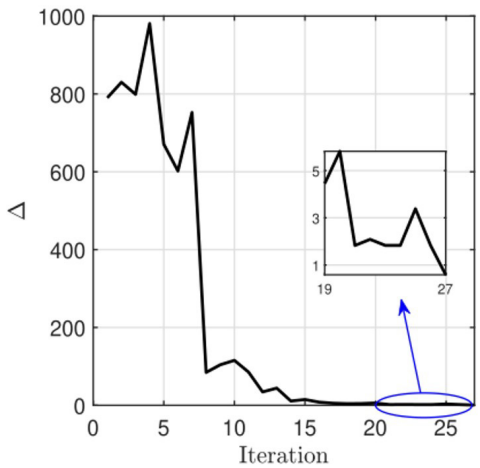

Figure 10: Convergence of differential evolution algorithm for the damped structure.

The optimal values $r_i = 0.137$ mm and $r_e = 4$ mm were found when damping was taken into account for the unit cell dynamics. The optimization clearly generates a region of strong attenuation as indicated by the shaded region in Fig. 11. This region corresponds to a band gap defined by the threshold value (14).

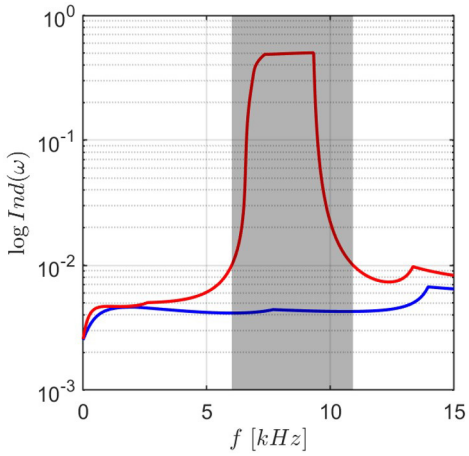

Figure 11: Evanescence index for the initial design (—) and optimal structure (—), when damping is taken into account. Figure in logarithmic scale.

It is interesting to note that the radius of the sphere is the same that was obtained in the undamped case. On the other hand, the beam radius is approximately 1.04% greater than previously found for the undamped structure. Within engineering precision, these values are practically the same and it is possible to conclude that the structural damping incurred due to $\eta = 1\%$ has no significant effect on the optimal solution found for the investigated structure. However, even in this case, damping can have significant influence in the range and intensity of attenuation. As shown in Fig. 12, no waves could propagate in the frequency range 6360-9006 Hz for the optimal undamped unit cell, whereas the zone of strong attenuation in the optimal damped structure comprises the frequency range 6020-10920 Hz. The addition of damping broadened the width of the band gap at the cost of a decreased peak of attenuation, a fact that has been observed in (Van Belle et al., 2017) through a case study, but not by optimizing a damped structure.

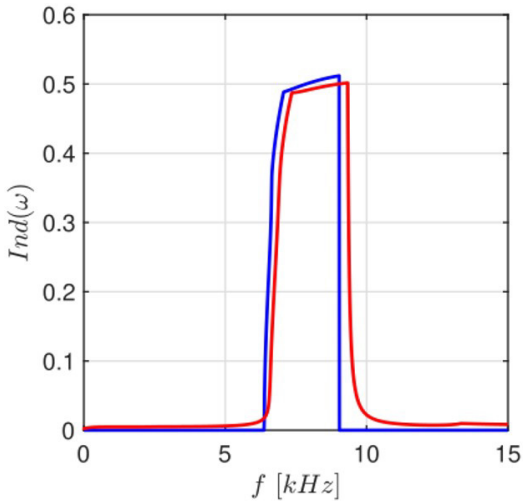

Figure 12: Evanescence index for optimal solutions considering the undamped (—) and damped (—) cases.

5.4 Consideration of a finite structure

The results of the optimizations are now verified for a finite structure composed of 20 unit cells, which is shown in Fig. 13 (only the resonator-free configuration is shown). It is expected that, as long as a sufficient number of unit cells are considered, the finite structure can exhibit similar wave attenuation behavior to that found for the infinite periodic structure (Hussein et al., 2006; Andreassen and Jensen, 2013), at the cost that wave propagation is strongly attenuated but not completely forbidden inside a band gap (Pierce and Matlack, 2021).

No geometrical restrictions are imposed at this stage (free boundary conditions). Different harmonic base motions are imposed on the left interface of the structure, which is shaded in blue. Corresponding transmitted motion is measured at the subsequent nodes, numbered 1-20. Nodes 1-19 (colored in black) are internal and node 20 (colored in red) is located at the right (free) interface. For example, if a base motion is imposed along y, then the y component of the displacement is measured for that point, and so on for x and z components. The torsional transmissibility, in particular, was assessed by imposing a rotation of the left interface about the z axis, and the corresponding rotation was measured for the indicated point at the right interface. This procedure was repeated four times, to account for the damped and undamped optimal structures, with and without local resonator.

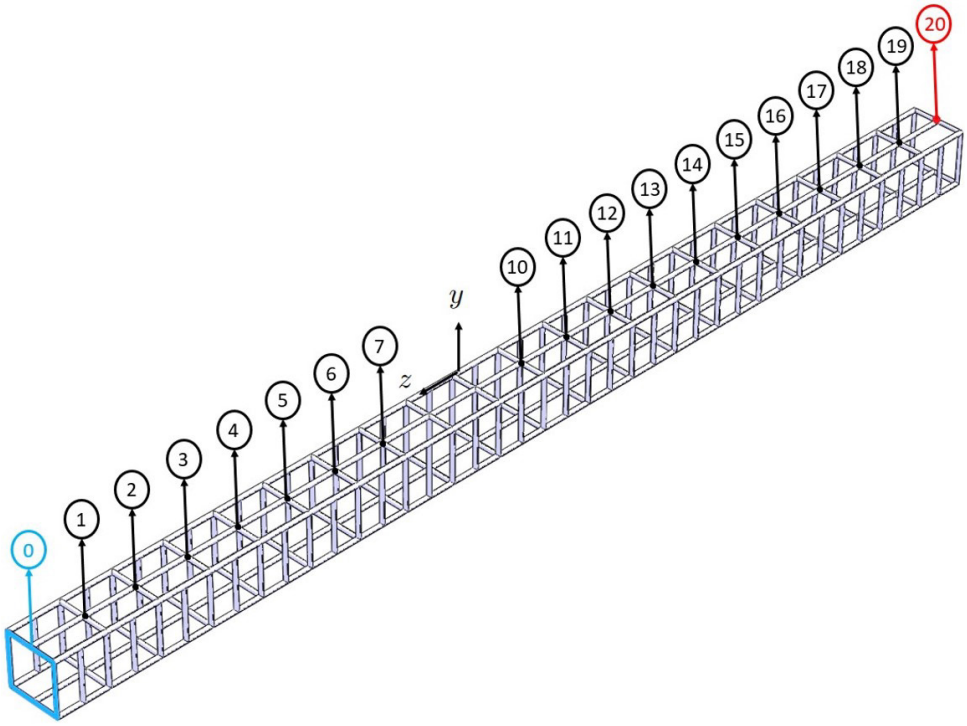

Figure 13: Finite structure with 20 unit cells with nodes 0-20. Numbering of nodes 8 and 9 has been omitted. The left interface, where base motions are applied, is colored in blue.

Again, the optimal undamped structure is considered first. Fig. 14 shows the transmissibility of motions from node 0 to the rightmost node 20. In this figure, the shaded region indicates the complete band gap predicted by wave theory, but it is important to analyze the peculiarities pertaining to each wave mode. Fig. 14a depicts the transmissibility for bending motion along the y axis. The dispersion relation indicates that the band gap for this mode starts at 3585 Hz, which is roughly the value indicated in the transmissibility plot. A similar situation arises when analyzing the transmissibility result for the bending motion along x and for the longitudinal motion (along z), shown in Figs. 14b and 14c, respectively. Since the torsional wave mode was the last to open a band gap, the region of reduced transmissibility is narrow, as indicated in Fig. 14d. It is also worthwhile to note the resonant peaks inside the shaded regions in Figs. 14a, 14b, and 14c. These peaks appear because the periodicity of the arrangement of unit cells is broken: the structures that are simulated are finite and their interfaces act as defects. This induces the formation of defect modes associated with mechanical resonance of the defect in the band gap regime, where evanescent waves are confined and energy localized (Jo et al., 2020; Bigoni et al., 2013). These defect modes cannot be avoided in finite structures, but even in their presence Fig. 14 indicates the gain of using local resonance to reduce vibration transmission when compared to the resonator-free counterpart.

Now, consider the optimal damped finite structure. Fig. 15 compares the transmissibility of motions from node 0 across to the rightmost node 20 for the damped and undamped cases. Figs. 15a, 15b and 15d indicate that bending and torsional modes have been significantly affected by the presence of damping, which broadened the width of the band gap and smoothed the peaks of attenuation. Curiously, Fig. 15c indicates the longitudinal mode is only slightly affected by the presence of damping. It should be noted that defect modes appear even in the presence of damping.

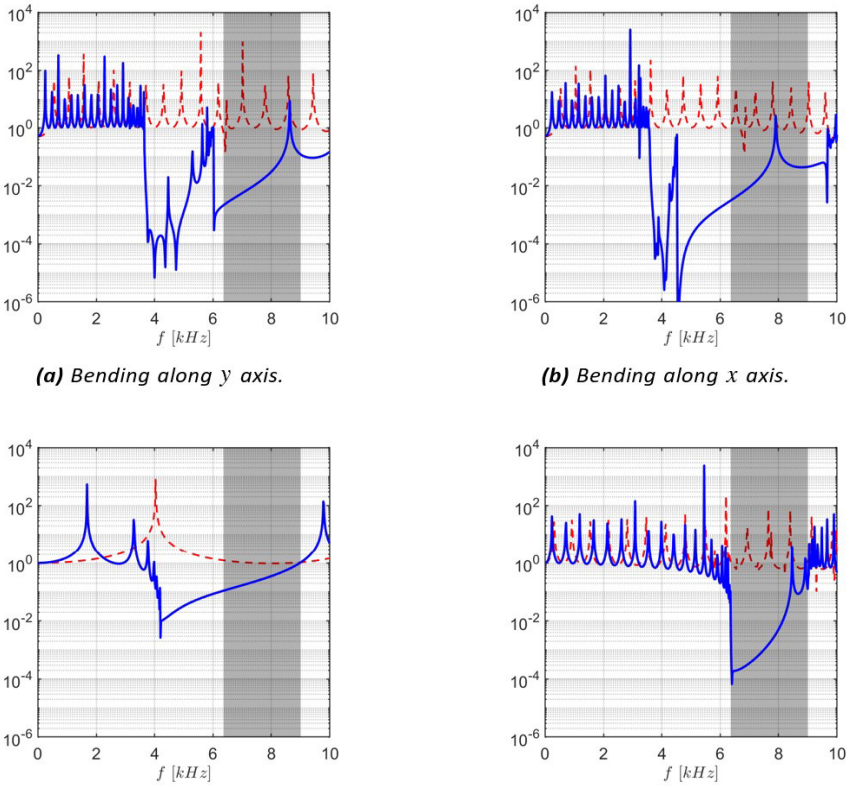

(a) *Bending along y axis.* ***(b)*** *Bending along x axis.*

(c) *Longitudinal motion.* ***(d)*** *Torsional motion.*

Figure 14: Transmissibility of different displacement modes for undamped finite structure made up of 20 unit cells. The plots show comparisons between the structure with localized resonators (—) and its resonator-free counterpart (—). The shaded area indicates the predicted complete band gap. The effect of other mode-specific band gaps can also be seen in the various plots.

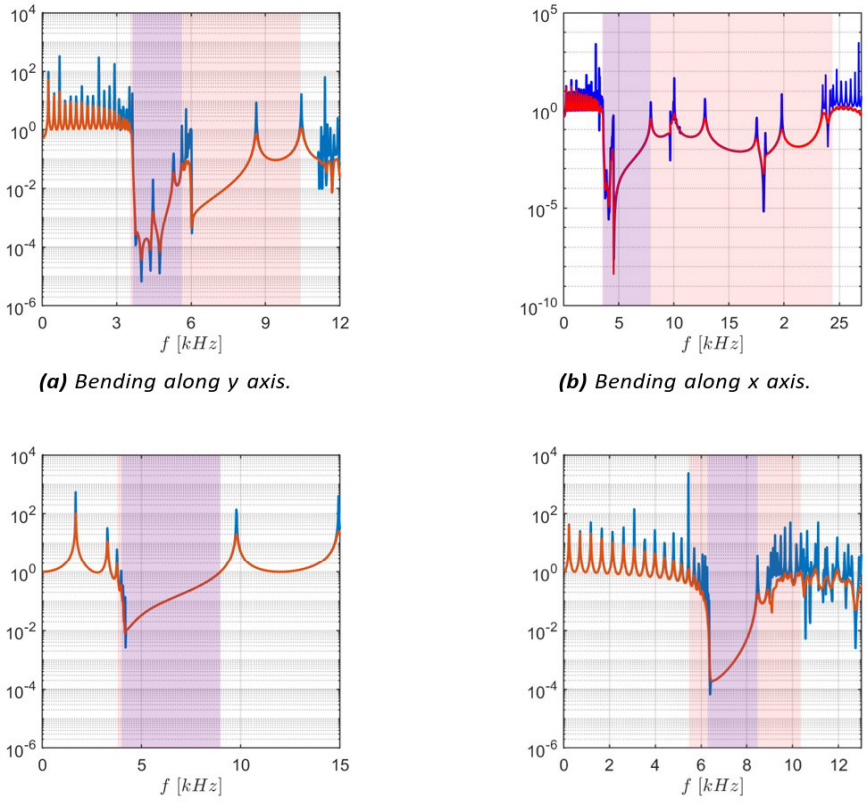

(a) *Bending along y axis.* ***(b)*** *Bending along x axis.*

(c) *Longitudinal motion.* ***(d)*** *Torsional motion.*

Figure 15: Transmissibility of different displacement modes for undamped (—) and damped (—) finite metamaterials. The area shaded in light blue corresponds to the zone of attenuation for the undamped material, and light red shading to the damped one.

A more complete picture of the finite metamaterials transmissibilities is provided when the displacements of nodes distributed along the beam length are considered, for frequencies found inside and outside the previously identified band gaps. Figs. 16 to 19 show the propagation of the four aforementioned types of motion along the optimal undamped and damped finite structures. In each graph, the ratio between amplitudes of nodes 1 to 20 with respect to the amplitude of node 0 (where motion was inputted) are plotted, as well as the corresponding phase shift. In the undamped case, the motion of the nodes is either in phase or 180º out of phase with respect to the imposed motion. For frequencies inside the zone of attenuation, motion decays spatially across the wave propagation direction for both cases. On the other hand, motion can be amplified for frequencies outside the zones of attenuation.

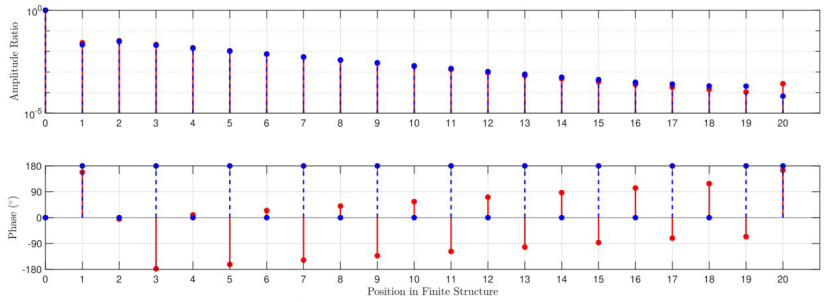

(a) *Motion for different nodes at 6400 Hz (inside band gap).*

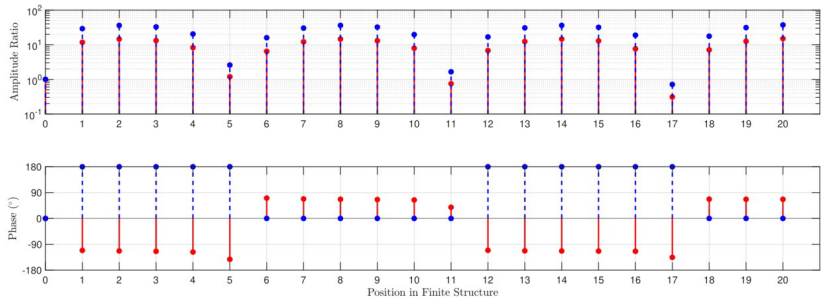

(b) *Motion for different nodes at 1666 Hz (outside band gap).*

Figure 16: Propagation of torsional motion across finite structure for undamped (—) and damped (—) optimal solutions.

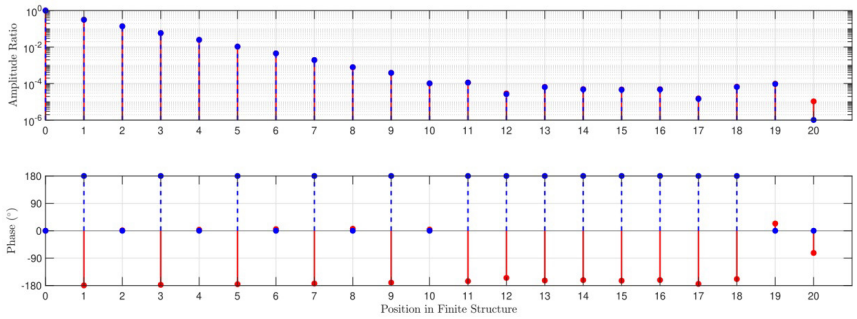

(a) *Motion for different nodes at 4080 Hz (inside band gap).*

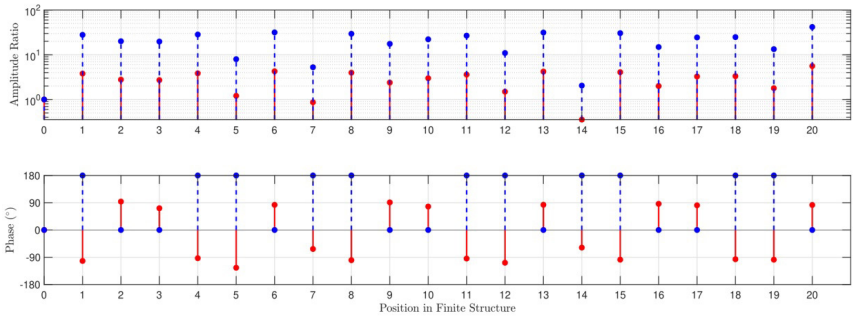

(b) *Motion for different nodes at 2516 Hz (outside band gap).*

Figure 17: Propagation of bending motion (along x axis) across finite structure for undamped (—) and damped (—) optimal solutions.

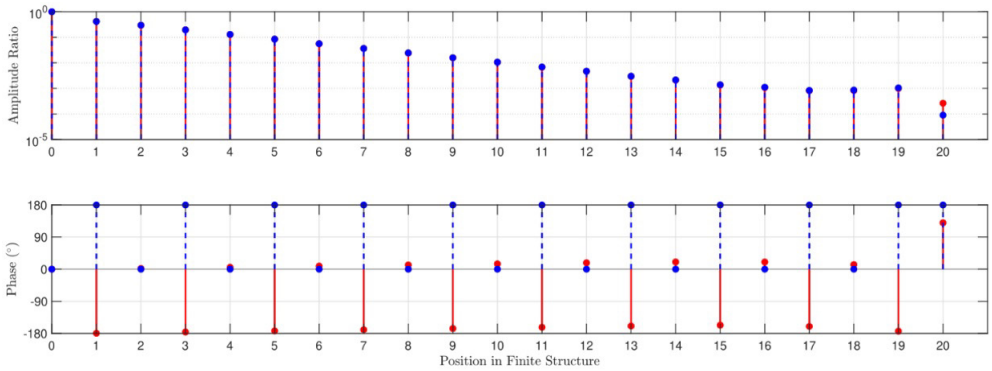

(a) *Motion for different nodes at 3780 Hz (inside band gap).*

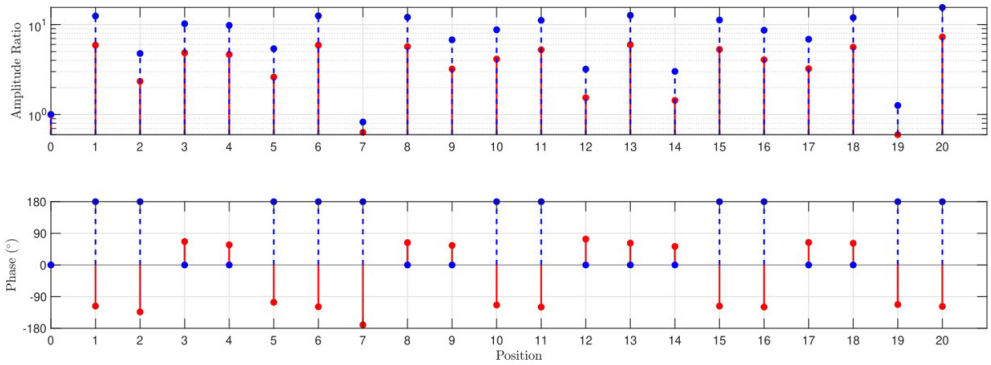

(b) *Motion for different nodes at 1833 Hz (outside band gap).*

Figure 18: Propagation of bending motion (along *y* axis) across finite structure for undamped (—) and damped (—) optimal solutions.

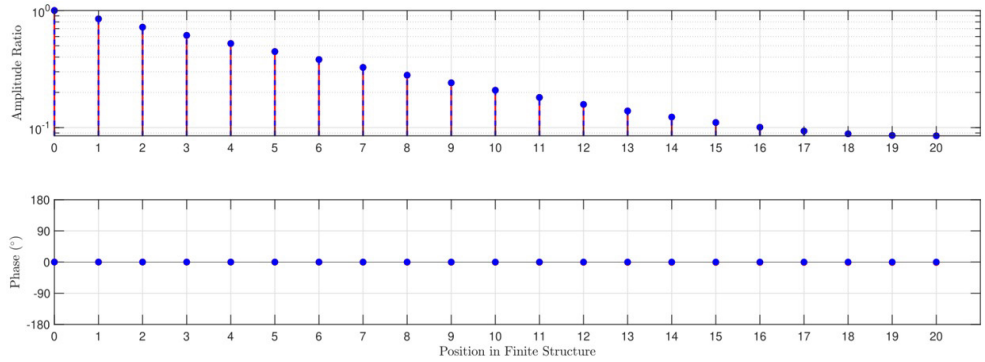

(a) *Motion for different nodes at 6000 Hz (inside band gap).*

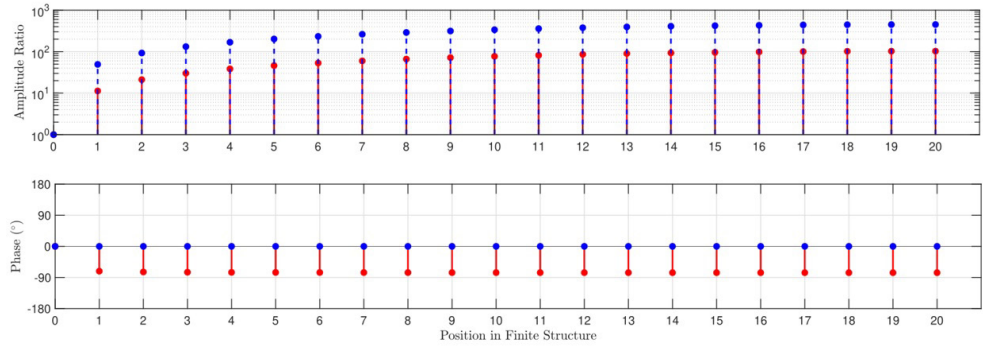

(b) *Motion for different nodes at 1683 Hz (outside band gap).*

Figure 19: Propagation of longitudinal motion across finite structure for undamped (—) and damped (—) optimal solutions.

6 CONCLUSIONS

A three-dimensional structure which shows one-dimensional periodicity and incorporates localized resonators was optimized to obtain wider band gaps in a lower frequency range when compared to its resonator-free counterpart. The structure was modeled with finite element and a comparison in design methodology was conducted for the cases when damping is present or not. The wave propagation characteristics were determined using the wave-based finite element method. When dissipation is not present, band gaps were identified directly from dispersion relations, since they correspond to frequency ranges where wave numbers are complex or imaginary. When damping was included, band gaps were identified as zones of intense attenuation, through an evanescence index.

The design parameters chosen for band gap optimization were the radii of the internal beams and of the sphere, which are related to the local resonances. A parametric analysis revealed that band gaps are widest for an intermediate value of beam radius: its increase and decrease shift the observed band gap to the right or left, respectively, while also making it narrower. Similarly, it was shown that the investigated band gap is wider for larger spheres: if it is not large enough, a band gap might not appear at all. When damping is included, the assessment of parametric influences has to be conducted by taking into account the adopted objective function, which incorporates an evanescence index, because band gaps are not as easy to visualize — since all wave modes are attenuated at every frequency.

Two optimization schemes were implemented, each reflecting whether the structure was damped or undamped. For the undamped case, a well-known objective function that maximizes band gap width and minimizes its central frequency was used. This objective function was modified to find optimal band gaps in damped elastic metamaterials, because application of its original form does not ensure the generation of frequency ranges characterized by strong wave attenuation. To that end, an evanescence index integral was incorporated in its denominator. While initial designs allowed wave propagation in the 0-10 kHz range, optimization opened band gaps in 6360-9006 Hz for the undamped case and 6020-10920 Hz for the damped one. However, peaks of attenuation are greater in the undamped case. From the design viewpoint, it is worth noting that this result conforms to previous notions that damping broadens width of the band gaps at the cost of a decreased peak attenuation. The optimization procedure was validated numerically for finite structures comprising twenty unit cells each, one without and the other with material damping. For both instances, free boundary conditions were assumed, and harmonic motion was imposed on one of their interfaces. By calculating the corresponding harmonic motion at the opposite interface, it was shown that regions of reduced transmissibility were introduced for bending, longitudinal and torsional modes. Bending and torsional modes have been significantly affected by the presence of damping, which broadened the width of the introduced band gap, and smoothed the peaks of attenuation. Curiously, the longitudinal mode was only slightly affected by the presence of damping. In addition, it was also shown that motion decays spatially for frequencies inside the zone of attenuation, while it can be amplified for frequencies outside the zones of attenuation.

In conclusion, the localized resonators of a damped elastic metamaterial were successfully optimized by a differential evolution algorithm. The proposed modified objective function produced zones of strong attenuation in lower frequency ranges, which introduced decreased transmissibility of mechanical waves over a wide range of frequencies. This demonstrates the potential utility of the investigated elastic metamaterial in diverse applications requiring vibration suppression, specially when compared to its resonator-free counterpart.

Acknowledgements

Authors would like to acknowledge the financial support provided by Fundação de Amparo à Pesquisa do Estado de São Paulo (FAPESP, grants #2018/15894-0 and #2020/06022- 0). D.A. Rade acknowledges the Conselho Nacional de Desenvolvimento Científico e Tecnológico (CNPq) (grant #312068/2020-4).

Author's Contributions: Conceptualization, R. G. Salsa Jr., T. P. Sales and D. A. Rade; Methodology, R. G. Salsa Jr., T. P. Sales and D. A. Rade; Investigation, R. G. Salsa Jr., T. P. Sales and D. A. Rade; Writing - original draft, R. G. Salsa Jr., T. P. Sales and D. A. Rade.

Editor: Marco L. Bittencourt and Josué Labaki

REFERENCES

Abedi, K., Mirjalili, S. M. (2015). Slow light performance enhancement of Bragg slot photonic crystal waveguide with particle swarm optimization algorithm. Optics Communications 339: 7–13.

Aladwani, A., Nouh, M. (2020). Mechanics of metadamping in flexural dissipative meta- materials: analysis and design in frequency and time domains. International Journal of Mechanical Sciences 173: 105459.

Andreassen, E., Jensen, J. S. (2013). Analysis of phononic bandgap structures with dissipation. Journal of Vibration and Acoustics 135.

Bacigalupo, A., Gnecco, G., Lepidi, M., Gambarotta, L. (2017). Optimal design of low-frequency band gaps in anti-tetrachiral lattice meta-materials. Composites Part B: Engineering 115: 341–359.

Bacigalupo, A., Gnecco, G., Lepidi, M., Gambarotta, L. (2019). Machine- learning techniques for the optimal design of acoustic metamaterials. Journal of Optimization Theory and Applications 187:630–653.

Baravelli, E., Ruzzene, M. (2013). Internally resonating lattices for bandgap generation and low-frequency vibration control. Journal of Sound and Vibration 332:6562–6579.

Bibi, A., Liu, H., Xue, J., Fan, Y., Tao, Z. (2019). Manipulation of the first stop band in periodically corrugated elastic layers via different profiles. Wave Motion 88:205–213.

Bigoni, D., Guenneau, S., Movchan, A. B., Brun, M. (2013). Elastic metamaterials with inertial locally resonant structures: application to lensing and localization. Phys. Rev. B 87:174303.

Bilal, Pant, M., Zaheer, H., Garcia-Hernandez, L., Abraham, A. (2020). Differential evolution: a review of more than two decades of research. Engineering Applications of Artificial Intelligence 90:103479.

Chen, Y., Guo, D., Li, Y. F., Li, G., Huang, X. (2019). “Maximizing wave attenuation in viscoelastic phononic crystals by topology optimization”. Ultrasonics 94:419–429.

Claeys, C. C., Deckers, E., Pluymers, B., Desmet, W. (2016). A lightweight vibro-acoustic metamaterial demonstrator: numerical and experimental investigation. Mechanical Systems and Signal Processing 70-71:853–880.

Collet, M., Ouisse, M., Ruzzene, M., Ichchou, M. N. (2011). Floquet–Bloch decomposition for the computation of dispersion of two-dimensional periodic, damped mechanical systems. International Journal of Solids and Structures 48:2837–2848.

Dal Poggetto, V. F., Bosia, F., Miniaci, M., Pugno, N. M. (2021). Optimization of spider web-inspired phononic crystals to achieve tailored dispersion for diverse objectives”. Materials & Design 209:109980.

Dal Poggetto, V. F., Arruda, J. R. F. (2021). Widening wave band gaps of periodic plates via shape optimization using spatial fourier coefficients. Mechanical Systems and Signal Processing 147: 107098.

Dal Poggetto, V. F., Serpa, A. L. and Arruda, J. R. F. (2019). “Optimization of local resonators for the reduction of lateral vibrations of a skyscraper”. In: Journal of Sound and Vibration 446, pp. 57–72.

Elmadih, W., Syam, W. P., Maskery, i., Chronopoulos, D., Leach, R. (2019). Multidimensional phononic bandgaps in three-dimensional lattices for additive manufacturing. Materials 12:1878.

Frazier, M. J., Hussein, M. I. (2012). Dissipation-triggered phenomena in periodic acoustic metamaterials. Proc. SPIE 8348, Health Monitoring of Structural and Biological Systems 2012, 83481W:523–531.

Gao, P., Climente, A., S’anchez-Dehesa, J., Wu, L. (2019). Single-phase metamaterial plates for broadband vibration suppression at low frequencies. Journal of Sound and Vibration 444:108–126.

Gazonas, G. A., Weile, D. S., Wildman, R., Mohan, A. (2006). Genetic algorithm optimization of phononic bandgap structures”. International Journal of Solids and Structures 43:5851–5866.

Han, X. K., Zhang, Z. (2019). Topological optimization of phononic crystal thin plate by a genetic algorithm. Scientific Reports 9:1–13.

Hussein, M. I., Hamza, K., Hulbert, G. M., Saitou, K. (2007). Optimal synthesis of 2D phononic crystals for broadband frequency isolation. Waves in Random and Complex Media 17:491–510.

Hussein, M. I., Hamza, K., Hulbert, G. M., Scott, R. A., Saitou, K. (2006). Multiobjective evolutionary optimization of periodic layered materials for desired wave dispersion characteristics. Structural and Multidisciplinary Optimization 31:60–75.

Hussein, M. I., Frazier, M. J. (2010). “Band structure of phononic crystals with general damping. Journal of Applied Physics 108:093506.

Jia, Z., Chen, Y., Yang, H., Wang, L. (2018). Designing phononic crystals with wide and robust band gaps. Physical Review Applied 9:044021.

Jo, S., Yoon, H., Shin, Y. C., Choi, W., Park, C., Kim, M., Youn, B. D. (2020). Designing a phononic crystal with a defect for energy localization and harvesting: supercell size and defect location. International Journal of Mechanical Sciences 179:105670.

Jung, J., Goo, S., Kook, J. (2020). Design of a local resonator using topology optimization to tailor bandgaps in plate structures. Materials & Design 191:108627.

Krushynska, A. O., Kouznetsova, V. G., Geers, M. G. D. (2016). Visco-elastic effects on wave dispersion in three-phase acoustic metamaterials. Journal of the Mechanics and Physics of Solids 96:29–47.

Liu, Z., Zhang, X., Mao, Y., Zhu, Y. Y., Yang, Z., Chan, C. T., Sheng, P. (2000). Locally Resonant Sonic Materials. Science 289:1734–1736.

Liu, Z., Wu, B., He, C. (2014). Band-gap optimization of two-dimensional phononic crystals based on genetic algorithm and FPWE. Waves in Random and Complex Media 24:286–305.

Van Belle, L., Claeys, C. C., Deckers, E., Desmet, W. (2017). On the impact of damping on the dispersion curves of a locally resonant metamaterial: modelling and experimental validation”. Journal of Sound and Vibration 409:1–23.

Matlack, K. H., Bauhofer, A., Kr¨odel, S., Palermo, A., Daraio, C. (2016). Composite 3D-printed metastructures for low-frequency and broadband vibration absorption. Proceedings of the National Academy of Sciences 113:8386– 8390.

Mencik, J. (2010). On the low-and mid-frequency forced response of elastic structures using wave finite elements with one-dimensional propagation. Computers &Structures 88:674–689.

Miranda Jr., E. J. P., Dos Santos, J. M. C. (2019). Flexural wave band gaps in multi- resonator elastic metamaterial Timoshenko beams. Wave Motion 91:102391.

Miranda Jr., E. J. P., Nobrega, E. D., Ferreira, A. H. R., Dos Santos, J. M. C. (2019). “Flexural wave band gaps in a multi-resonator elastic metamaterial plate using Kirchhoff-Love theory”. Mechanical Systems and Signal Processing 116:480–504.

Pierce, C. D., Matlack, K. H. (2021). “Fuzzy band gaps”: a physically motivated indicator of bloch wave evanescence in phononic systems. Crystals 11.

Romero-García, V., S’anchez-P’erez, J. V., Garc’ıa-Raffi, L. M., Herrero, J. M., Garc’ıa-Nieto, S., Blasco, X. (2009). Hole distribution in phononic crystals: design and optimization. The Journal of the Acoustical Society of America 125:3774–3783.

Vasileiadis, T., Varghese, J., Babacic, V., Gomis-Bresco, J., Urrios, D. N., Graczykowski, B. (2021). Progress and perspectives on phononic crystals”. Journal of Applied Physics 129:160901.

Vatanabe, S. L., Paulino, G. H., Silva, E. C. N. (2014). Maximizing phononic band gaps in piezocomposite materials by means of topology optimization. The Journal of the Acoustical Society of America 136:494–501.

Wang, Y., Wang, Y. (June 2013). complete bandgap in three-dimensional holey phononic crystals with resonators. Journal of Vibration and Acoustics 135.

Xiao, X., He, Z. C., Li, E., Cheng, A. G. (2019). Design multi-stopband laminate acoustic metamaterials for structural-acoustic coupled system. Mechanical Systems and Signal Processing 115:418–433.

Xiao, Y., Wen, J., Wen, X. (2012). Longitudinal wave band gaps in metamaterial- based elastic rods containing multi-degree-of-freedom resonators. New Journal of Physics 14:033042.

Zhang, H., Xiao, Y., Wen, J., Yu, D., Wen, X. (2015). Flexural wave band gaps in metamaterial beams with membrane-type resonators: theory and experiment. Journal of Physics D: Applied Physics 48:435305.

Zhong, W. X., Williams, F. W. (1995). On the direct solution of wave propagation for repetitive structures. Journal of Sound and Vibration 181:485–501.